A&A 513, A71 (2010)
DOI: 10.1051/0004-6361/200912022

Astronomy & Astrophysics

Echo outbursts in KS 1731–260

V. Šimon

Astronomical Institute, Academy of Sciences of the Czech Republic, 251 65 Ondřejov, Czech Republic
e-mail: simon@asu.cas.cz

Received 10 March 2009 / Accepted 17 December 2009

ABSTRACT

Context. The thermal-viscous instability of the accretion disk is thought to play an important role in the activity of low-mass X-ray binaries (LMXBs). It should also appear when a (quasi)persistent LMXB goes into its low state.
Aims. We analyze the long-term X-ray activity of the neutron star LMXB KS 1731–260 during a part of its long main outburst and a complicated transition back to the low state (quiescence). We pay special attention to the variations during the state transition.
Methods. We make use of the ASM/*RXTE* observations for a timeseries analysis of the longterm variations and investigation of the X-ray color changes in the 1.5–12 keV passband.
Results. In our interpretation, the mass transfer rate $\dot{m}_{\rm tr}$ between the donor and neutron star significantly increased during the main outburst of KS 1731–260, which prolonged this event by keeping the disk ionized to its outer rim. Later on, a considerable fraction of the outer part of the disk was rapidly brought out of steady-state when $\dot{m}_{\rm tr}$ decreased again. Only a slow decrease of $\dot{m}_{\rm tr}$ continued even after the end of the main outburst. This lead to the formation of the central disk region, which was kept thermally stable, ionized by irradiation, and was surrounded by the outer, thermally unstable disk region. This configuration triggered the series of the echo outbursts. These outbursts are outside-in, caused by the still continuing $\dot{m}_{\rm tr}$ via the mass stream impinging the outer rim of the disk without overflow. We argue that introducing any strong bursts of matter from the donor to the disk as the cause of the echo outbursts is superfluous. The spectral evolution suggests that the disk returns to steady-state during the maxima of the echo outbursts. The X-ray emission between the echo outbursts is much higher than in the true quiescence and can be due to the ongoing $\dot{m}_{\rm tr}$. We place the peculiar long-term activity of KS 1731–260 in the context of the systems with the echo outbursts, both soft X-ray transients and dwarf novae.

Key words. stars: neutron – accretion, accretion disks – novae, cataclysmic variables – circumstellar matter – X-rays: binaries – stars: individual: KS 1731–260

1. Introduction

Low-mass X-ray binaries (LMXBs) are generally classified either as persistent or transient X-ray sources according to their long-term X-ray behavior (e.g. Lewin et al. 1995). Transient sources called soft X-ray transients (SXTs) are observed to display occasional outbursts, during which their X-ray flux rises typically by several orders of magnitude (e.g. Chen et al. 1997). These outbursts are separated by intervals of quiescence considerably longer than the outbursts themselves. These sources are very faint in quiescence, and some may be below the detection limit of the available X-ray instruments. Their activity is interpreted in terms of the thermal-viscous instability of the accretion disk (e.g. Dubus et al. 2001), similar to that in dwarf novae (DNe) (e.g. Warner 1995). On the other hand, persistent sources are repeatedly detected by X-ray instruments, and their X-ray flux varies by a factor of few. Their disks appear to be steady-state on the hot branch of the so-called S-curve, i.e. the flow of matter through the disk is constant and the disk rapidly reacts to the variations of the mass inflow from the donor.

An important question arises as to whether transients can change into persistent sources and vice versa during the time interval covered by our X-ray satellites (i.e. during several decades at most, on a much shorter time scale than the evolutionary one). The second question regards the process of such a change, i.e. whether it is abrupt or gradual and if there are any observable properties which precede and herald it. In the framework of the thermal-viscous instability, the mass transfer rate between the donor and the compact accretor appears to be the key factor.

Currently, we know about several LMXBs that behaved like persistent X-ray sources for an interval of several years and then their X-ray flux decreased by a considerable amount (KS 1731–260 (Wijnands et al. 2001a); X1732–304 (Wijnands et al. 2002a); 4U 2129+47 (Wijnands 2002; Nowak et al. 2002); 1M 1716–315 (Jonker et al. 2007)). Cyclic variations resembling outbursts with the recurrence time $T_{\rm C} \approx 46$ days also appeared in 4U 1636–53 when the X-ray luminosity of this system decreased. Nevertheless, it has not reached the quiescence yet (Shih et al. 2005).

KS 1731–260 is a remarkable system, as regards its long-term activity. It turned on in 1988 (Syunyaev et al. 1990; Chelovekov et al. 2006) and remained in the high state for ~12.5 years. This can be characterized as a triple main outburst with the true quiescence between the peaks either absent or significantly shorter than the duration of the outbursts. King (2006) classified KS 1731–260 as an on/off transient that stayed in the high state for several years. It contains a neutron star (NS) because it displayed several X-ray bursts (Syunyaev et al. 1990). Wijnands et al. (2001a) attributed the X-ray emission in quiescence detected with *Chandra* to the cooling NS, not to accretion. The luminosity of this object continued to decrease even in quiescence (Wijnands et al. 2002b). The distance determined from the X-ray burst is $d \approx 7$ kpc (Muno et al. 2000). The source is characterized by variable intrinsic absorption (Barret et al. 1998). The optical candidate (Orosz et al. 2001a; Wijnands et al. 2001a; Mignani et al. 2002) is of an intermediate spectral type, but its luminosity class is uncertain. It is consistent with the LMXB nature of KS 1731–260 (Barret et al. 1998).

The orbital period $P_{\rm orb}$ is unknown, but Revnivtsev & Sunyaev (2003) interpreted a cycle of about 38 days in the main outburst in terms of the disk precession. By analogy with Her X-1, they estimated $P_{\rm orb}$ to be 1–3 days.

In this paper we analyze the long-term evolution of the X-ray activity of KS 1731–260. We pay particular attention to the outbursts accompanying the transition to quiescence. We also investigate the X-ray color variations and their role in the assessment of the relation of the main outburst to the so-called echo outbursts. We place the activity of KS 1731–260 in the context of the echo outbursts in both SXTs and DNe.

2. Observations

Recent activity of KS 1731–260 between 1996–2005 was observed by the All Sky Monitor (ASM) onboard the *Rossi X-ray Timing Explorer* (*RXTE*) (Levine et al. 1996) (http://xte.mit.edu/). Our analysis considers only this time interval, since the observations after JD 2 451 800 are consistent with the system being under the detection limit of ASM/*RXTE*. The data file used here contains the sum band intensities $I_{\rm sum}$ in the 1.5–12 keV passband and the hardness ratios $HR1 = I_{\rm B}(3{-}5\ {\rm keV})/I_{\rm A}(1.5{-}3\ {\rm keV})$, $HR2 = I_{\rm C}(5{-}12\ {\rm keV})/I_{\rm B}(3{-}5\ {\rm keV})$. Since our analysis concentrates on variations on timescales of days and longer, we used the one-day means and their errors $\sigma_{\rm q}$ provided by the ASM/*RXTE* team.

PCA data (2–60 keV) from the Galactic center scans adopted from Wijnands et al. (2001a) were included, too. In order to display them along with ASM observations, their intensities were re-calculated using the countrate of the Crab nebula; 1 Crab is approximately 13 000 ct s^{-1} PCA (2–60 keV) (Shirey et al. 1996). However, the bulk emission lies in the 2–20 keV passband. On the other hand, 1 Crab = 75 ct s^{-1} of ASM/*RXTE*. Scaling of these PCA data was thus made by a division of their countrate by 13 000 ct s^{-1} and multiplication by 75 ct s^{-1}. This means that PCA data were not simply renormalized to some feature in ASM observations.

3. Data analysis

3.1. The overview

The whole sum band ASM/*RXTE* light curve of KS 1731–260 is displayed in Fig. 1a, while the zoomed part of the interval with the large fluctuations is shown in Fig. 1b. The observations started shortly before the time of the peak flux (hereafter called main outburst). This peak was followed by a slow decline, until large-amplitude variations (hereafter called echo outbursts) appeared near JD 2 451 000. The observations after JD 2 451 800 are consistent with the system being below the detection limit.

The ASM data set was submitted for a detailed visual inspection. It was revealed that some data display a large $\sigma_{\rm q}$ and thus introduce a large noise level. It was therefore decided to set the truncation limit of $\sigma_{\rm q}$ of $I_{\rm sum}$ at 2 ct s^{-1}. This significantly improved the light curves. At the same time, the coverage remained sufficiently dense. In order to lower the scatter of the observations, to emphasize the slowly varying component of the X-ray variations and to pick out their profile, the data were fitted by the code called HEC13 written by Prof. Harmanec. The code is based on the method of Vondrák (1969, 1977), who improved the original method of Whittaker (Whittaker & Robinson 1946). The method is based on minimizing the value $Q = F + \lambda^2 S$, where $F = \sum p(y_{\rm i} - y'_{\rm i})^2$ denotes the degree of smoothing (y being the smoothed and y' the observed value of the variable), $S = \sum(\Delta^3 y_{\rm i})^2$ is the measure of roughness of the curve, λ^2 is a constant to be selected and defines how much the curve will be smoothed. A full description of the method can be found in Vondrák (1969). This method can fit a smooth curve to the nonequidistant data no matter what their profile is. HEC13 makes use of two input parameters, ϵ (in dimensionless units) and ΔT. The quantity $\epsilon = 1/\lambda^2$ determines how "tight" the fit will be, that is, if only the main profile or also the high-frequency variations are to be reproduced. The quantity ΔT is the interval over which the data are binned before smoothing. The resulting fit consists of the mean points, calculated to the individual observed points of the curve. A set of fits to the ASM data with the different ϵ and ΔT was generated and submitted to inspection. It was found that the fit with $\epsilon = 10^{-1}$, $\Delta T = 5$ d reproduces the main features of the profile of ASM light curve and suppresses the rapid fluctuations. This fit picks out only those features that are defined by multiple data points. It is true that this method is somewhat subjective, but it enables us to find a compromise between a curve running through all the observed values and an ideal smooth curve. We preferred to use this method because it does not make any assumptions about the profile of the fitted data. The X-ray curves of SXTs are often complicated (e.g. Chen et al. 1997), so a considerable part of information could be lost by fitting a particular function.

Fluctuations of $I_{\rm sum}$ on the timescale of days can preclude the profile of the changes on a long timescale, particularly if the amplitudes of these variations are comparable to each other. In order to investigate the long-term evolution of $I_{\rm sum}$, the data were also smoothed by the two-sided moving averages. The filter half-widths $Q = 60$ and 90 d in steps of 5 d were used; Q refers to the semi-interval within which the data were averaged (Fig. 1a).

An overview of the dramatic X-ray changes can be obtained from the statistical distribution of $I_{\rm sum}$ (Fig. 2). To follow its evolution with time, the ASM data were divided into several segments. It can be clearly seen that the distribution of $I_{\rm sum}$ is almost symmetric in the main outburst, although the mean flux slightly varies. A remarkable change occurred when the large-amplitude fluctuations of $I_{\rm sum}$ started. The mean flux decreased, while the amplitude of the flux variations increased. Also the profile of the distribution, especially its skewness, underwent a considerable change. The mean intensity between the echo outbursts was clearly above $I_{\rm sum} = 0$ ct s^{-1}. The flux is compatible with the nondetection of the system after JD 2 451 831. Its occasional excursions up to ~3 ct s^{-1} can be explained by a noise and fluctuations of the background.

3.2. Evolution of the echo outbursts

The time evolution of the echo outbursts can be investigated by an analysis of the evolution of their basic parameters (Fig. 3). They were determined from the HEC13 fits to the light curve as described in Sect. 3.1 and displayed in Fig. 1. In our analysis, the segment of the echo outbursts begins by the edge of the slowly decaying light curve of the main outburst in JD 2 451 051. The peak intensity of the echo outburst, $I_{\rm max}$, tends to decrease with time, no matter if it was measured in JD or in the epoch E (Fig. 3a,b). Figure 3c shows the decay rates of the echo outbursts measured in ct s^{-1}. The slopes of these decaying branches were determined from a linear fit to each well-mapped branch. Although the real profile is more complicated in some cases, a linear approximation was found to be plausible for our purposes. The same approach was also applied to the steep, final decline of the main outburst near JD 2 451 060. In Fig. 3d the skewness is a measure of asymmetry of the outburst light curve. It depends

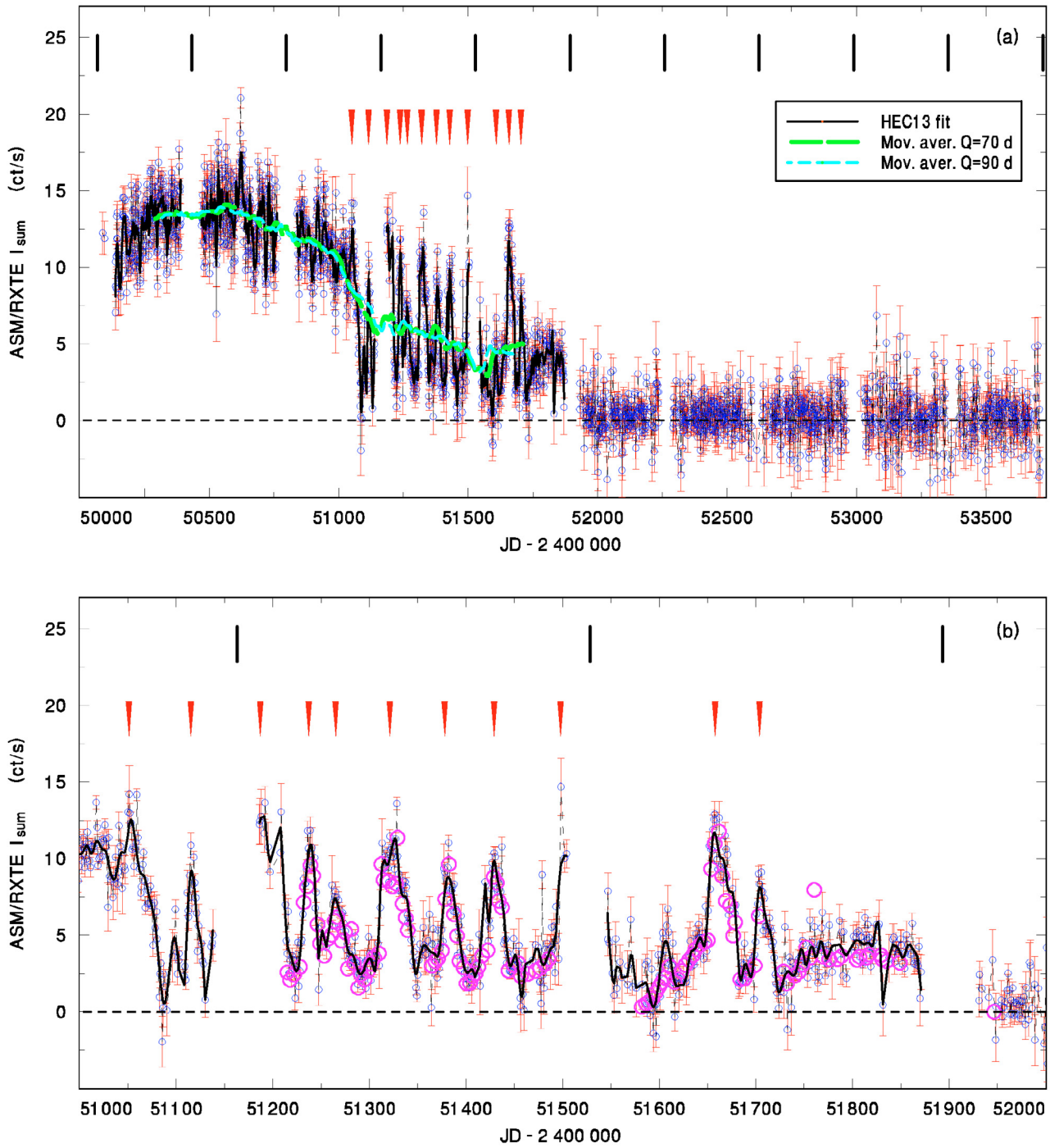

Fig. 1. Long-term X-ray light curve of KS 1731–260. The whole curve is shown in **a)**, while the zoomed part with the echo outbursts is displayed in **b)**. Small open circles represent the ASM/*RXTE* sum band (1.5–12 keV) one-day means; they are connected by a line for the densely covered segments. The uncertainties quoted in the original file of ASM measurements are marked. The two-sided moving averages of the one-day means for various values of Q, measured in days, are included in **a)**. Large open circles in **b)** denote PCA observations (Wijnands et al. 2001a) with the intensity re-scaled to match ASM data, as described in Sect 2. Smooth solid line represents the fit to ASM data by the code HEC13. Triangles denote the outburst maxima used for our analysis (i.e. those with the maximum of the fitted curve $I_{\rm sum} > 7$ ct s^{-1}). Short vertical lines mark the conjunction of the system with the Sun. See Sect. 3.1 for details. (This figure is available in color in electronic form.)

mainly on three parts of the profile – the rising branch, the shape and duration of the peak flux, and the decaying branch. The values of skewness >0 and <0 correspond to the asymmetric distributions with a tail toward higher or lower values of $I_{\rm sum}$ than the mean, respectively. Most outbursts possess a skewness of larger than zero, which means that the rising branch is faster than the decaying branch.

When comparing the energy output of the individual outbursts in a given system (e.g. SXT), we can get a better insight if we introduce the fluence of the outburst. It was calculated by integration of the 1.5–12 keV X-ray light curve of the outburst fitted by HEC13. It thus represents the area outlined by the outburst light curve in the investigated passband. The limits of this integration (the start and finish of the outburst) were set equal to

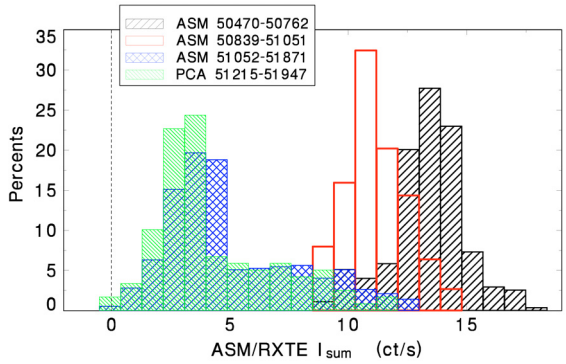

Fig. 2. The statistical distribution of $I_{\rm sum}$ in KS 1731–260. HEC13 fits and PCA data from Fig. 1 are used. The segment between the time of the peak flux and finish of the echo outbursts is considered. Notice that the decrease of the mean flux is accompanied by a large variation of the skewness. The flux is compatible with the nondetection of the system after JD 2 451 831. See Sect. 3.1 for details.

$I_{\rm sum} = 0$ ct s^{-1}, even when the intensity between these outbursts remained above 0 ct s^{-1}. The fluence thus represents the energy output of each outburst in a given energy passband. Since we are interested in comparing the relative outputs only in a given SXT the fluence may be expressed in dimensionless units (Fig. 3e). The time evolution of the ratio of the fluence to the outburst duration D, given in dimensionless units, is plotted in Fig. 3f.

It can be seen in Fig. 1b that most echo outbursts are discrete and separated from each other. The peaks of most individual events can therefore easily be resolved. It appears promising to apply the method of the O–C residuals, successfully tested on DNe and SXTs (Vogt 1980; Šimon 2000; Šimon 2002; Šimon 2004). This method enables us not only to determine the recurrence time $T_{\rm C}$, but also to analyze its variations. It works with the residuals from some reference period (i.e. with the deviations from a constant period). This method is not sensitive to the exact length of the reference period. A slightly different reference period produces only an additional linear trend of the O–C curve, which can be corrected later. The relation between the O–C curve and $T_{\rm C}$ is as follows: a linear profile of the O–C curve, no matter what its slope, implies a constant $T_{\rm C}$. A parabolic profile of the O–C curve implies a linear change of $T_{\rm C}$ ($T_{\rm C}$ is increasing/decreasing if the parabola is curved upward/downward). The resulting O–C curve also enables us to assess the position of each outburst with respect to the O–C profile of the remaining outbursts. This method can work even if some outbursts are missing due to the gaps in the data, provided that the profile of the O–C curve is not too complicated. It is known that $T_{\rm C}$ of DNe and SXTs can vary by a large amount. The standard period searches therefore often reveal nothing. Nevertheless, the O–C curves still show that in many cases the changes of $T_{\rm C}$ are not chaotic, and the well-defined trends can be resolved in the O–C diagrams.

Only the clearly defined echo outbursts with the maximum of the fitted curve $I_{\rm sum} > 7$ ct s^{-1} were considered. Since most these outbursts were found to possess sharp peaks, the times of their maxima could be determined quite precisely, with a typical error of 1–2 days. This is always considerably smaller than their recurrence time $T_{\rm Ceo}$, as shown below.

In order to obtain some starting value of $T_{\rm Ceo}$, a separation between consecutive outbursts was determined. The resulting O–C curve with an almost horizontal profile of most

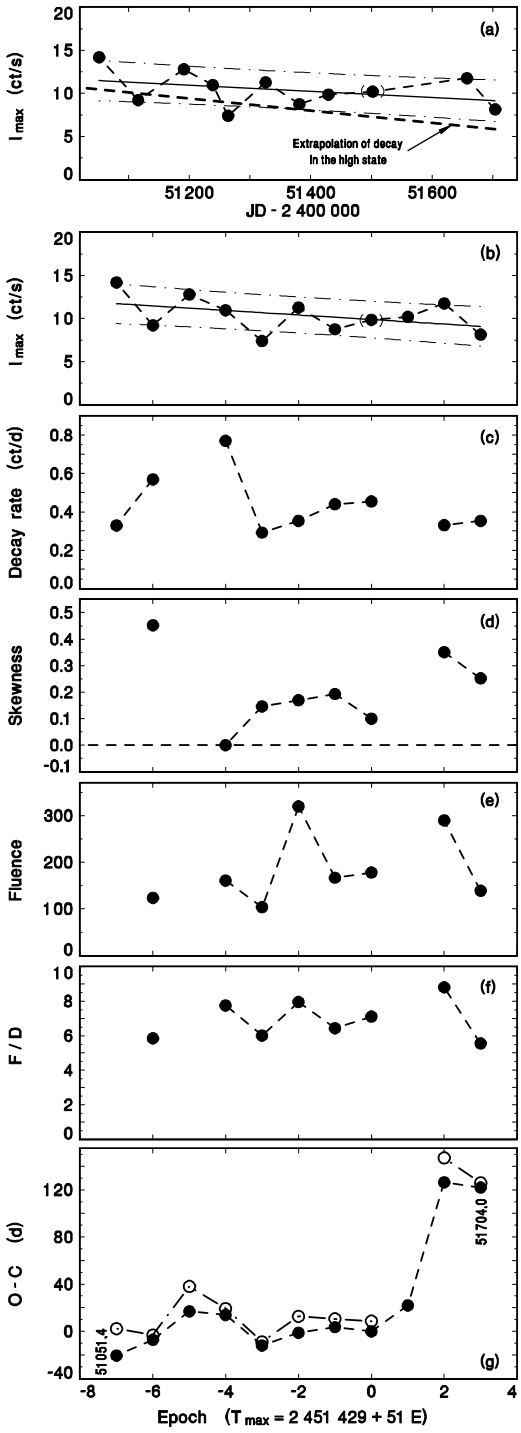

Fig. 3. Time evolution of the parameters of the echo outbursts in KS 1731–260. They were determined from the HEC13 fits shown in Fig. 1. **a)** Variations of $I_{\rm max}$ vs. JD. An insecure value is marked by the brackets. A linear fit and its standard deviation are displayed. The thick dashed line represents an extrapolation of the decaying branch of the main outburst. **b)** Variations of $I_{\rm max}$ with epoch E. **c)** Decay rates of the echo outbursts. The steep decline of the main outburst is included in $E = -7$. **d)** Skewness of the echo outburst. **e)** Fluence of the echo outburst. **f)** Ratio of fluence to the outburst duration (in dimensionless units). **g)** O–C diagram for $T_{\rm Ceo}$ of the echo outbursts. The times of $I_{\rm max}$ are marked by solid circles. The times of crossing $I_{\rm sum} = 7$ ct s^{-1} on the decaying branch are denoted by open circles. The numbers at some points represent the times of the outburst maxima in JD–2 400 000 for convenience. The outbursts that can be considered as consecutive, that is without gaps in the data, are connected by dashed lines. See Sect. 3.2 for details.

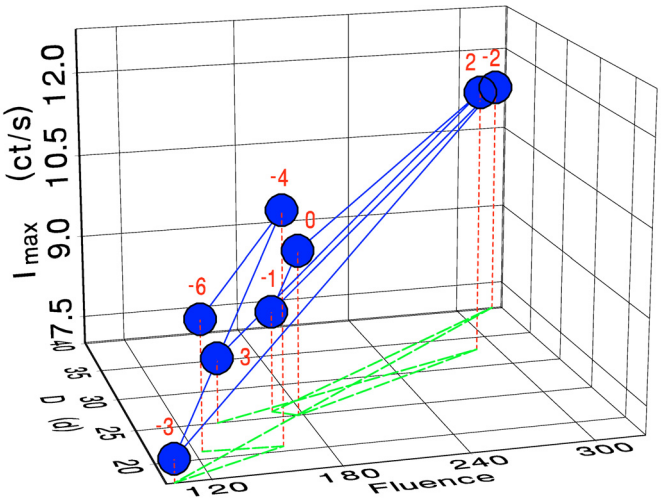

Fig. 4. The relation between D, fluence, and I_{max} of the echo outbursts in KS 1731–260. These parameters were determined from HEC13 fits. The numbers at the points denote E according to Eq. (1). The points are connected by a line to show the time evolution. See Sect. 3.2 for details.

points is displayed in Fig. 3g. It was calculated according to the ephemeris in Eq. (1)

$$T_{max} = 2\,451\,429 + 51\,E. \quad (1)$$

Only a few events need an explanation. The series of the maxima of the echo outbursts begins at the edge of the slowly decaying light curve of the main outburst in JD 2 451 051. Notice that its position in the O–C curve of the outburst maxima also plausibly agrees with the O–C curve of the decaying branches (Fig. 3g). Further, the HEC13 fit shows small brightenings with the maxima in JD 2 451 100 and JD 2 451 607. It is very difficult to decide if they are real outbursts or only fluctuations of I_{sum} between the outbursts. We do not take these events as outbursts because their maxima are below our limit of $I_{sum} > 7$ ct s^{-1}. In addition, the PCA data in Fig. 1 display only a small feature in their gradual increase of intensity between JD 2 451 582 and JD 2 451 650, which casts doubts on the reality of the outburst in JD 2 451 607.

The relation between fluence, D of the echo outburst, and its I_{max} in KS 1731–260 is displayed in Fig. 4. These parameters were determined from the HEC13 fits. For convenience, the numbers at the points denote E according to Eq. (1). Although some scatter is apparent in this relation, it can be seen that both a brighter and longer echo outburst is needed to obtain a bigger fluence of the event. Examples of the profile of the echo outburst are displayed in Fig. 5. Notice that their rising branch is steeper than the decaying one, as also indicated by the skewness >1 of most events. The statistical distribution of the decay rates determined above is displayed in Fig. 6. The main slope of the decrease of I_{sum} in all the events displayed in Fig. 6 turns out to be 0.43 ± 0.15 ct d^{-1}.

3.3. X-ray hardness

The X-ray color variations of KS 1731–260 were analyzed using $HR1$ and $HR2$. When plotted versus I_{sum}, the curves of both $HR1$ and $HR2$ were found to contain several points with quite large errors in HR. In order to lower the noise, the points which had the quoted uncertainty of their $HR \geq 0.3$ were rejected. Secondly, to resolve the mean profile of the $HR1$ and $HR2$ curves, they were

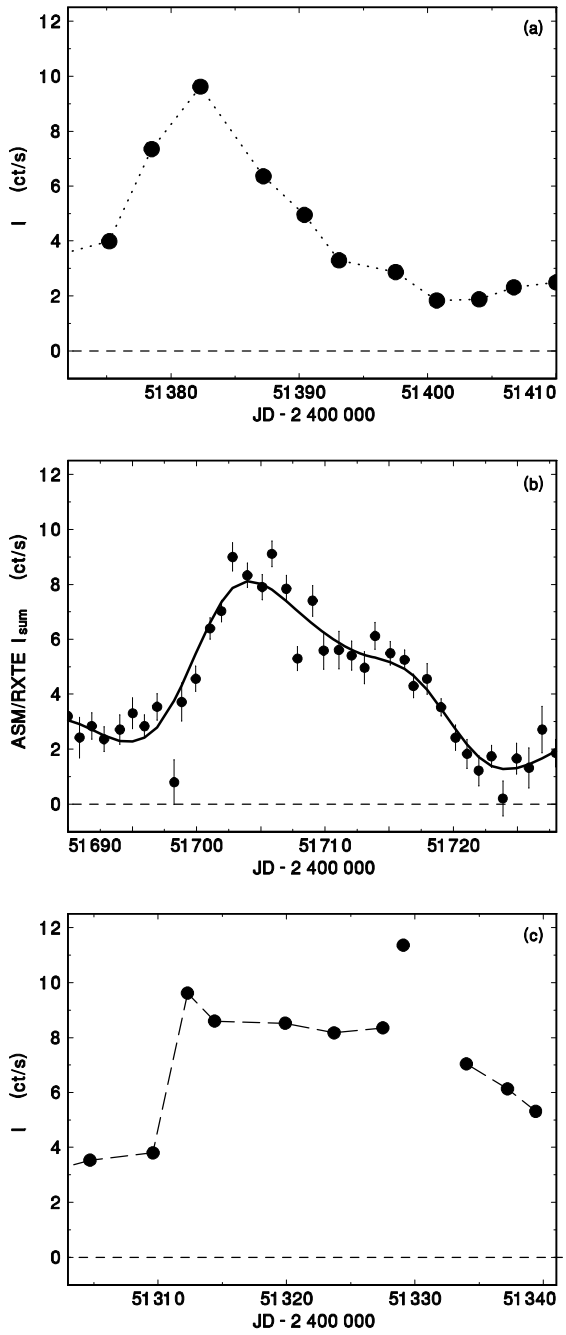

Fig. 5. **a)** Example of the echo outburst with a sharp peak in KS 1731–260. PCA data with the intensity re-scaled to match the ASM data are used. The points are connected by a line for clarity. **b)** Example of the profile of the echo outburst with a broken profile of the decline (ASM data). The HEC13 fit is marked by a solid line. **c)** Light curve of a flat-topped echo outburst (PCA data with the intensity re-scaled to match the ASM data). The scales of the axes are identical for all three panels. See Sect. 3.2 for details.

fitted as a function of I_{sum} by HEC13. The fits with the parameters $\epsilon = 1$, $\Delta I_{sum} = 3$ ct s^{-1} were proven to satisfy the data. This fit was truncated at $I_{sum} = 17$ ct s^{-1}, because the amounts of data were too low to enable a reliable fit above this limit. The dependence of $HR1$ and $HR2$ on I_{sum} is displayed in Fig. 7. Three states are resolved: main outburst, echo outbursts, quiescence between the echo outbursts. The thick smooth lines represent the HEC13 fits to the whole data set. It is obvious that a monotonic function was obtained for $HR1$, with significantly

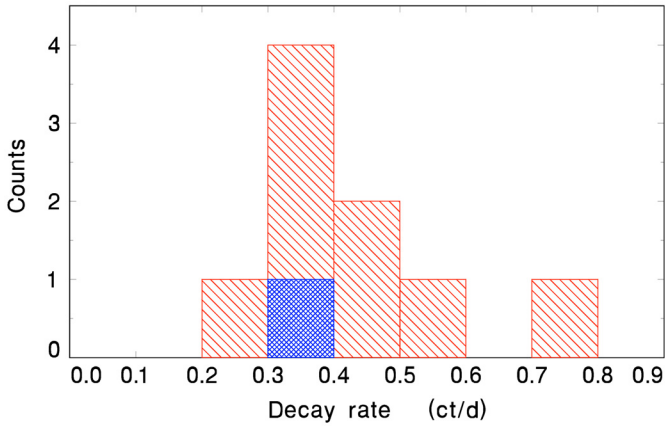

Fig. 6. The statistical distribution of the decay rates of outbursts in KS 1731–260. The distribution for the ensemble containing the echo outbursts + the final, steep decline of the main outburst is marked by tilted lines. The steep decline of the main outburst is denoted by the box filled by crosses. ASM data are used. See Sect. 3.2 for details.

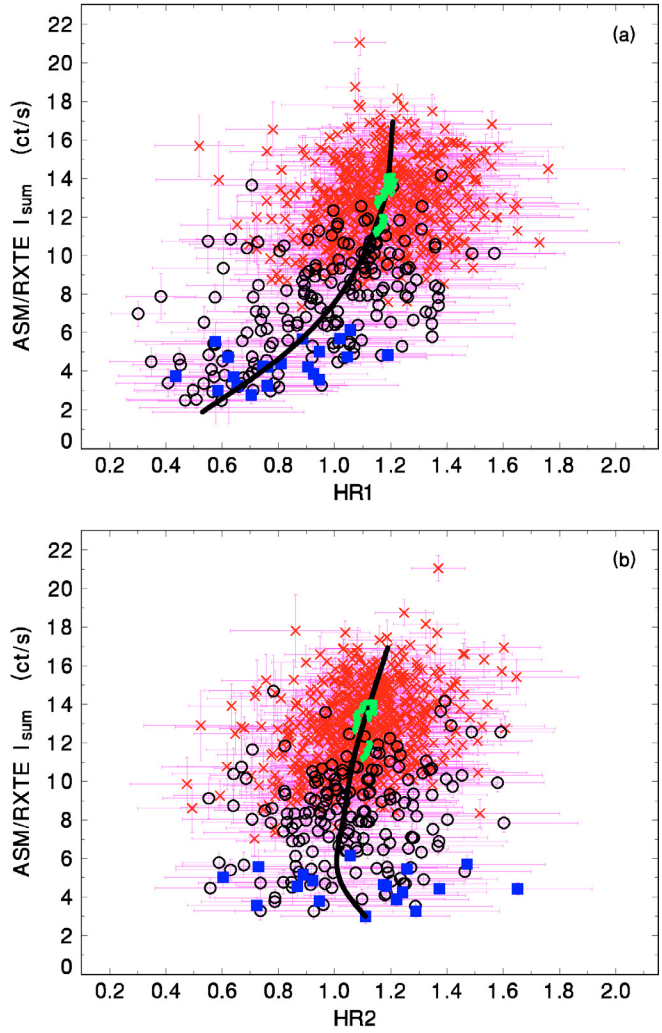

Fig. 7. *HR*1 and *HR*2 vs. $I_{\rm sum}$ in KS 1731–260. The scales of the axes are identical for both diagrams. Three states of activity are resolved: main outburst (crosses), echo outbursts (open circles), quiescence between the echo outbursts (solid boxes). The thick smooth lines represent the HEC13 fits to the whole data set. Small inverted triangles along HEC13 fit represent the long-term evolution during the main outburst smoothed by the two-sided moving averages. See Sect. 3.3 for details. (This figure is available in color in electronic form.)

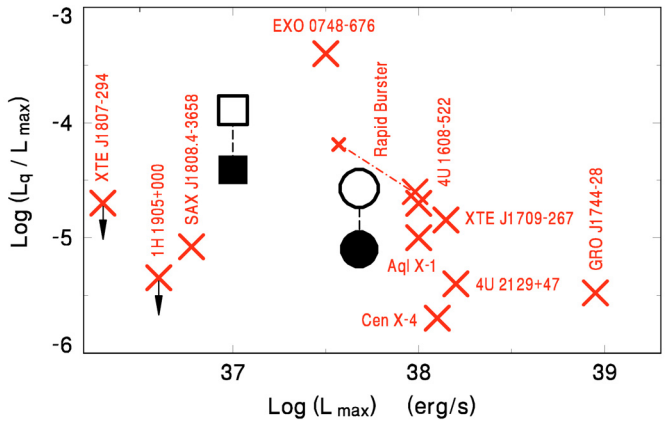

Fig. 8. The peak luminosity $L_{\rm max}$ vs. the ratio of the quiescent and peak luminosity of NS SXTs. The names are given for convenience. The large open and solid circles denote the position of KS 1731–260 for $L_{\rm q}$ measured in March 27, 2001, and September 13, 2001, respectively. The large open and solid boxes denote the position of KS 1731–260 for the same $L_{\rm q}$ as the circles, but they utilize the luminosity between the echo outbursts instead of $L_{\rm max}$. The outbursts of group A (large cross) and group B (small cross) are displayed for the Rapid Burster (Šimon 2008). See Sect. 3.4 for details. (This figure is available in color in electronic form.)

smaller *HR*1 for the smallest $I_{\rm sum}$ (Fig. 7a). On the other hand, the profile of *HR*2 is more complicated (Fig. 7b); *HR*2 reaches a minimum at $I_{\rm sum} \approx 6$ ct s^{-1} and slightly increases toward both larger and smaller $I_{\rm sum}$. To investigate the long-term evolution of *HR* vs. $I_{\rm sum}$ in the main outburst, the data were smoothed by the two-sided moving averages with the filter half-width $Q = 80$, 90, 100 and 110 days, in steps of 5 days. Since the individual fits agree well with each other, only the fit for $Q = 80$ d is shown in Fig. 7.

3.4. Luminosity of KS 1731–260 in the context of NS SXTs

Plotting the peak luminosity $L_{\rm max}$ of outburst vs. $L_{\rm q}/L_{\rm max}$ of NS SXTs ($L_{\rm q}$ denotes the quiescent luminosity) can help us to assess if and how the properties of KS 1731–260 differ from those of SXTs. For KS 1731–260, we plot $L_{\rm max}$ of the main outburst determined from the HEC13 fit. For comparison, also the typical position of KS 1731–260 for the luminosity between the echo outbursts instead of $L_{\rm max}$ is included; $I_{\rm sum} = 3$ ct s^{-1}, determined from Fig. 2, was used for this purpose. The resulting diagram (Fig. 8) is based on those by Narayan et al. (1997), Garcia et al. (1998), Robinson et al. (2002) and Šimon (2008). The position of Aql X-1 was re-calculated for $d = 4$ kpc (Rutledge et al. 2001). The luminosities of additional systems come from these authors: SAX J1808.4–3658 (in't Zand et al. 2001; Campana et al. 2002), 1H 1905+000 (Jonker et al. 2006), XTE J1807–294 (Campana et al. 2003; Campana et al. 2005), XTE J1709–267 (Jonker et al. 2003), GRO J1744–28 (Finger et al. 1996). For KS 1731–260, $L_{\rm max} \approx 7.9 \times 10^{37}$ erg s^{-1} was determined from the unabsorbed flux, derived by Wijnands et al. (2001a). The coefficients of extinction by Morrison & McCammon (1983) were used. The unabsorbed quiescent luminosity $L_{\rm q} \approx 1.6 \times 10^{33}$ erg s^{-1} was determined from the measurement on March 27, 2001, of Wijnands et al. (2001a). The luminosity $L_{\rm q}$ further decreased to $\sim 4.7 \times 10^{32}$ erg s^{-1} on September 13, 2001 (Wijnands et al. 2002b). Both positions of KS 1731–260 are displayed in Fig. 8.

Table 1. Systems with multiple (≥2) echo outbursts following the main outburst.

System	Type	P_{orb}	Outb. year	Passband	No. EO	Mean T_C (d)	T_m/T_{echo}	S	q
KS 1731–260	NS LMXB		1988	X	10	51	4.97	1.3	
SAX J1808.4–3658	NS SXT	2.0142 h [1]	2000	X, O [2, 3]	9	13	0.13	>1.5 [4]	~0.05 [4]
GRO J0422+32	BH SXT	5.0920 h [5]	1992	O [6]	2	137	0.71	70 [7]	0.12 [8]
GRS 1009–45	BH SXT	6.8449 h [9]	1993	O [10]	≥3	~25?	~1	24 [7]	0.14 [9]
XTE J1859+226	BH SXT	9.16 h [11]	1999	O [12]	≥3	27	2.30	115 [12]	
XTE J1550–564	BH SXT	37.248 h [13]	1998	X [13]	2	~320	0.37	2.8	<0.08 [13]
V4641 Sgr	BH HMXB	67.615 h [14]	1999	O, X [15, 16]	≥4	377 [17]	~0.1		0.67 [18]
V803 Cen	DN	0.44333 h [19]	2003	O [20]	≥9	0.8			0.08 : [21]
2003aw	DN	0.56568 h [22]	2004	O [22]	~5	~5			
WZ Sge	DN	1.3605 h [23]	2001	O [24]	12	1.7	0.83		0.09 [25]
EG Cnc	DN	1.4105 h [26]	1996	O [26]	6	7.3	0.45		
SDSS J080434+510349	DN	1.4167 h [27]	2006	O [28]	11	2.6			
UZ Boo	DN	1.4568 h [29]	2003	O [30]	~4	~3	0.68		

References. 1. Chakrabarty & Morgan (1998); 2. Wijnands et al. (2001b); 3. Wijnands (2006); 4. Deloye et al. (2008); 5. Chevalier & Ilovaisky (1994); 6. Callanan et al. (1995); 7. Chen et al. (1997); 8. Webb et al. (2000); 9. Filippenko et al. (1999); 10. Bailyn & Orosz (1995); 11. Filippenko & Chornock (2001); 12. Zurita et al. (2002); 13. Orosz et al. (2002); 14. Goranskij (2001); 15. Uemura et al. (2002); 16. Maitra & Bailyn (2006); 17. Šimon (2008); 18. Orosz et al. (2001b); 19. Roelofs et al. (2007b); 20. Kato et al. (2004); 21. Roelofs et al. (2007a); 22. Nogami et al. (2004); 23. Skidmore et al. (1997); 24. Patterson et al. (2002); 25. Steeghs et al. (2007); 26. Patterson et al. (1998); 27. Szkody et al. (2006); 28. Pavlenko et al. (2006); 29. Szkody (1987); 30. Henden (2008, priv. comm.).

3.5. KS 1731–260 in the context of the echo outbursts

Although the behavior observed during the transition from the main outburst in KS 1731–260 is rare, it is not quite unique among SXTs. Table 1 lists the systems with multiple echo outbursts (i.e. at least two such events in a single main outburst). It helps us place KS 1731–260 in the context. The type of the system and P_{orb} are given in Table 1 if they are known. Also the year of the start of the appropriate main outburst is listed. The passband in which the echo outbursts were observed (X. X-rays, O. optical) is given. Number EO refers to the number of the observed echo outbursts that follow the main outburst. The quantity T_m/T_{echo} is the ratio of the duration of the main outburst to the duration of the interval during which the echo outbursts were observed. In our notation, the echo outbursts are events that occur on the declining branch of the main outburst or shortly after its end. The duration of the series of the echo outbursts is considerably shorter than the quiescent time interval between the main outbursts. The highest ever observed number of the echo outbursts in a given outburst is given if more than one main outburst in a given system was accompanied by the echo outbursts. For SXTs, the quantity S was included; it is the ratio of the peak X-ray flux of the main outburst to the typical peak X-ray flux of the echo outburst or, alternatively, to the X-ray flux on the declining branch of the main outburst below which the echo outbursts started. The mass ratio is given in the form $q = M_c/M_{donor}$, where M_c and M_{donor} are the mass of the compact object and donor, respectively. Uncertain value is marked by :. The numbers in the squared brackets denote the references; if no number is given, the relevant value was determined by our analysis.

The relation between P_{orb} and the mean T_{Ceo} in the systems listed in Table 1 is displayed in Fig. 9. Plots in both log-log and linear scales are shown. The types of the systems are resolved (SXTs, WZ Sge-type DNe, ultra-compact DNe). Here the term ultra-compact DN is used for V803 Cen and 2003aw, which have an extremely short P_{orb}. Their donors thus must be smaller than main-sequence stars. It can be seen that the systems with very short P_{orb} like the SU UMa systems concentrate in a small range of short T_{Ceo}. Although the long P_{orb} systems with the echo outbursts are rare, their T_{Ceo} is really longer than in the SU UMa systems. Since P_{orb} of KS 1731–260 is unknown, its position is marked by the horizontal line to cover the range of P_{orb} of the investigated systems.

4. Discussion

We present the results of our analysis of a peculiar long-term X-ray activity in the NS LMXB KS 1731–260. They regard a part of its main outburst and a complicated transition back to quiescence (low state) (Fig. 1). The onset of a series of brightenings called the echo outbursts lead to a striking change of activity. We also show that although these echo outbursts fall into a group of features only rarely observed in some SXTs and DNe (Table 1), the activity of KS 1731–260 can be successfully placed in the context of these systems.

Soft X-ray luminosity of the main outburst in KS 1731–260 smoothed in time is the key factor that governs the presence or absence of the echo outbursts. These events started abruptly below $L_X \approx 3.7 \times 10^{37}$ erg s^{-1}, as determined from $I_{sum} \approx 11$ ct s^{-1} (Fig. 1). The level of the peak L_X is thus related to the level of the late phase of the slow decay of the main outburst.

Although a variety of profiles of outbursts in SXTs exists (e.g. Chen et al. 1997), only the exponential and linear decays can be treated by the available models (King & Ritter 1998; Dubus et al. 2001). They can already distinguish between two cases. In the former case, the whole disk is kept in the ionized state by irradiation. In the latter case, irradiation is able to keep only the inner disk region ionized, while the outer region is in the cool state, that is with the effective temperature below the critical one, T_{crit}. The quantity T_{crit} is the temperature below which the gas begins to recombine (e.g. Warner 1995). The slopes of the decaying branches of the individual subsequent echo outbursts in KS 1731–260 were definitely much steeper than those of the main outburst observed before JD 2 451 051. This suggests a large structural change of the disk. The outburst decay of SXT is predicted to steepen considerably when it changes from an exponential to a linear one. The quantity I_{max} of the individual

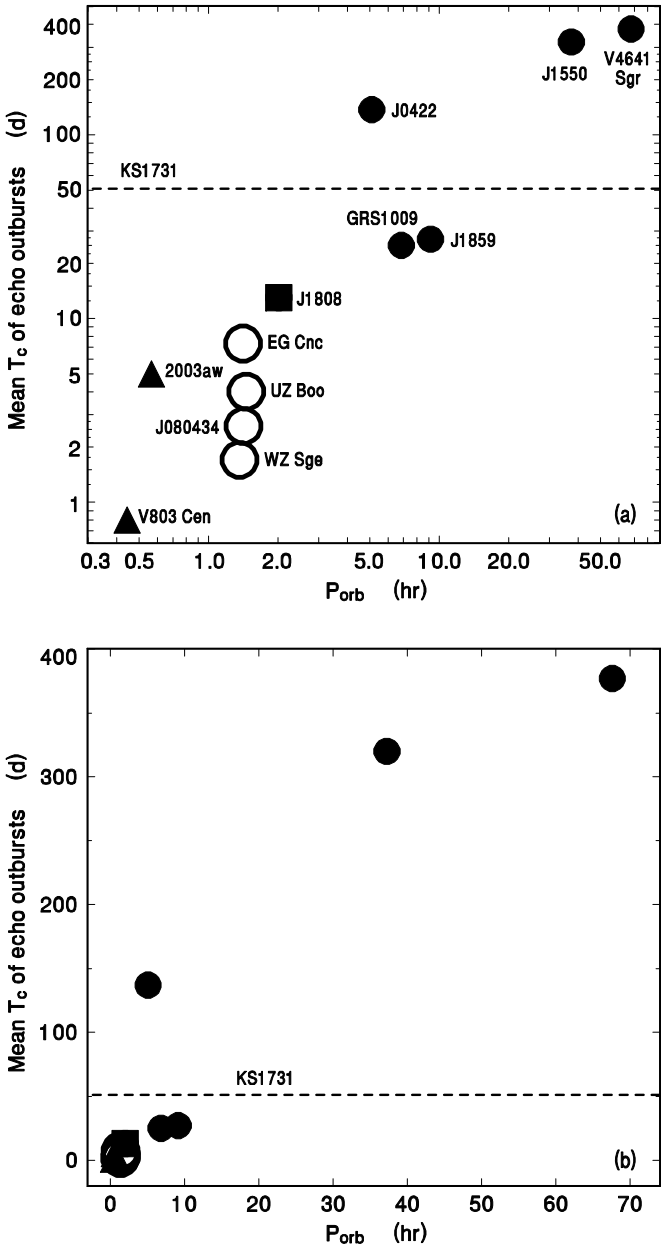

Fig. 9. The relation between $P_{\rm orb}$ and the mean $T_{\rm Ceo}$ of the echo outbursts in the systems listed in Table 1 (logarithmic **a)** and linear **b)** scale of the axes). The types of the systems are resolved: NS SXT – closed box, black hole SXTs – closed circles, WZ Sge-type DNe – open circles, ultra-compact DNe – closed triangles. The position of KS 1731–260 is marked by the horizontal line. See Sect. 3.2 for details.

echo outbursts is limited from above and is never much higher than the intensity of the end of the slow decline of the main outburst in JD 2 451 051 (Fig. 1). A big steepening of the slope of the decay is thus really observed when the profiles of the main outburst and of the individual echo outbursts are compared.

Nevertheless, the decay of the main outburst is far from being exponential even after smoothing. Also, its decay timescale until JD 2 451 051 (Fig. 1a), $\tau_{\rm d} \approx 1200$ d, falls far behind the upper end of the statistical distribution of the SXT outbursts. They peak at $\tau_{\rm d} \approx 25$ d in Chen et al. (1997). In view of this it is also important that KS 1731–260 displays the smallest S among SXTs in Table 1. All this suggests a very small depletion rate of the disk during the main outburst of KS 1731–260. Although its $P_{\rm orb}$ is unknown, it is reasonable to assume that the whole disk was in steadystate at this time. The model by Bath & Pringle (1981) shows that both the disk luminosity and structure settle down in a time considerably shorter than the observed main outburst. The observed very slow decay can be explained if the mass inflow rate from the donor to the disk, $\dot{m}_{\rm tr}$, becomes a significant fraction of the mass accretion rate from the disk onto the NS, $\dot{m}_{\rm acc}$ during the outburst (Eq. (9) in Powell et al. 2007). We assume the relation $L_{\rm X} = \eta \dot{m}_{\rm acc} c^2$, where $\eta \approx 0.1$ and c is the speed of light. This increased mass supply modifies the outburst profile and can cause the disk state to be governed by $\dot{m}_{\rm tr}$, if it is able to keep the disk effective temperature above $T_{\rm crit}$.

We thus interpret the onset of the echo outbursts in KS 1731–260 as a decrease of $\dot{m}_{\rm tr}$ to the level at which the temperature of the outer disk region decreases below $T_{\rm crit}$. The large amplitude of these fluctuations shortly after the end of the main outburst suggests that a considerable fraction of the outer part of the disk was rapidly brought out of steady-state. Indeed, the model of the time behavior of a disk whose mass inflow was abruptly reduced confirms that the instability rapidly propagates through the disk (King & Cannizzo 1998). Our interpretation is strengthened by the fact that the slope of the steep, final decline of the main outburst near JD 2 451 060 is consistent with those of the subsequent echo outbursts (Fig. 6). Introducing any bursts of matter from the donor to the disk as the cause of the echo outbursts is thus superfluous. The individual echo outbursts preserve a characteristic time scale of their variations, especially of the rise and decay. A bigger fluence is a result of a longer and brighter outburst, not due e.g. to the narrow, intense spikes (Figs. 6, 3f, 4). This suggests that similar and relatively large parts of the disk are involved in each outburst.

The skewness of the profiles of the echo outbursts in KS 1731–260 larger than zero suggests that these events possess a steeper rise than decay (Fig. 3d). As discussed above, their peak intensity is comparable to that of the end of the slow decay of the main outburst. The outside-in type of outbursts, caused by the still continuing $\dot{m}_{\rm tr}$ via the mass stream impinging the outer rim of the disk without overflow, can provide an explanation. The reason is that immediately after reaching $\Sigma_{\rm max}$ (the upper end of the cool branch of the S-curve Dubus et al. 2001) in the outer disk rim, the heating front begins to propagate inward. An alternative explanation by an optically thin ADAF, that makes the disk change into a torus and forces the outburst to be triggered far from the disk center even in the case of the mass stream overflow is unlikely in our case. The reason is that the disk did not get into a true low state between most echo outbursts, as suggested by the luminosity clearly above the true quiescent value and by HR smaller (softer) than or comparable to that of the main outburst (Fig. 7). The fact that the echo outbursts displayed a trend of a steady decrease of the peak intensity, but not of fluence, cannot be caused by any large spectral changes during the outburst. These changes could not shift a large part of the emission out of the passband of ASM, because HR varied only a little (Fig. 7).

The evolution of the X-ray spectrum of the whole event (main outburst and echo outbursts) traced in the HR vs. $I_{\rm sum}$ diagram (Fig. 7) allows us to conclude that the spectral profile at the peak of the echo outburst is consistent with that in the main outburst. The disk thus returns to steady-state during the maxima of these echo outbursts. The evolution of $HR1$ with $I_{\rm sum}$ (Fig. 7a) suggests that the X-ray spectrum softens with the decreasing intensity, while the opposite is expected if any optically thin advection-dominated accretion flow (ADAF, Narayan et al. 1997) forms when the disk is depleted by accretion. This

means that in KS 1731–260 the structure of the inner disk region between the echo outbursts is not very different from that in the main outburst and in the peak of the echo outburst. When heavily smoothed, the data of the main outburst follow the fit to the whole data set, so the X-ray spectrum of the main outburst becomes harder when the system brightens (Fig. 7). The evolution of $HR1$ and $HR2$ with $I_{\rm sum}$ bears a resemblance to that in the atoll system 4U 1820–30 (Šimon 2003) and indicates that KS 1731–260 is an atoll, too. This is another way of confirmation of the findings by Wijnands & van der Klis (1997) and Muno et al. (2000).

The position of KS 1731–260 in the $L_{\rm max}$ vs. $L_{\rm q}/L_{\rm max}$ diagram and its comparison with other SXTs (Fig. 8) are helpful in further discussion. The luminosity of KS 1731–260 observed between the echo outbursts is comparable to that of three systems at the fainter end of $L_{\rm max}$ (two millisecond pulsars with very short $P_{\rm orb}$ (Ritter & Kolb 2003) and an ultracompact candidate (Jonker et al. 2006)). We thus obtain $L_{\rm X} \approx 10^{37}$ erg s^{-1} and $\dot{m}_{\rm acc} \approx 10^{18}$ g s^{-1} ($1.7 \times 10^{-8}\ M_{\odot}$) in between the echo outbursts of KS 1731–260, assuming the same η. These values are by several orders of magnitude higher than in quiescent NS SXTs. All this suggests that the inner disk region of KS 1731–260 is still kept in the hot, ionized state, and is surrounded by the outer, thermally unstable disk region. Indeed, the thermal instability seems to be able to operate in such a configuration, as shown by the models of Mineshige et al. (1990) and Leach et al. (1999). Nevertheless, further modeling of such a configuration and the resulting time variations is needed.

The relatively smooth profiles of the O–C curves suggest that the individual echo outbursts are dependent on each other in KS 1731–260 (Fig. 3g). The amplitude of the superimposed outburst-to-outburst fluctuations is significantly smaller than that of the long-term profile of the O–C curve, hence of $T_{\rm Ceo}$. This quantity undergoes complicated nonmonotonic variations. Both the initial decrease of $T_{\rm Ceo}$ and the prominent increase in the late phase were observed. This profile cannot be explained by the action of a single one-way process, e.g. by only an increase/decrease of $\dot{m}_{\rm tr}$ or the disk viscosity. Both these mechanisms can be tested using our data. An increase of $\dot{m}_{\rm tr}$ is expected to give rise to a decrease of $T_{\rm C}$ accompanied by an increase of the peak luminosity of the outburst (e.g. the model by Hameury et al. 1998). This contradicts our observations. Variations of the disk viscosity between the echo outbursts can account for this time evolution of $T_{\rm Ceo}$. In this scenario, an initially small viscosity of the disk left after the main outburst explains why $T_{\rm Ceo}$ is initially longer than the mean. The viscosity then increases toward its approximately stable mean achieved in the middle segment. The final increase of $T_{\rm Ceo}$ suggests another decrease of the viscosity later on. The long quiescent interval preceding the echo outburst in $E = 2$ contains an episode of an exceptionally low $I_{\rm sum}$ centered on JD 2 451 590 (Fig. 1b). We interpret it as a shrinkage of the inner disk region between the echo outbursts, possibly due to a decrease of irradiation. The disk viscosity is lower in the cold state than in the hot state (e.g. Hameury et al. 1998; Dubus et al. 2001). A larger zone brought to the cool state thus requires more matter to accumulate in the disk to reach $\Sigma_{\rm max}$. This can then power a more energetic outburst, that is the one with a bigger fluence. The big fluence of the echo outburst in $E = 2$ preceded by an exceptionally long $T_{\rm Ceo}$ is in accordance with this scenario.

Our interpretation of the echo outbursts in terms of the thermal-viscous instability is also consistent with the behavior of KS 1731–260 in the earlier phases of its triple outburst. Although the TTM/KVANT light curve (Chelovekov et al. 2006) is fragmentary, it does show largeamplitude fluctuations between the peaks of the main outburst. We interpret them as the onset of the thermal instability caused by a decrease of $\dot{m}_{\rm tr}$. The first peak of the triple outburst lasted for ~400 days, which may still be marginally compatible with a "normal" outburst of SXT. The scenario for the subsequent two even broader peaks of the outburst is analogous to that proposed by Esin et al. (2000) for GRO J1655–40; the donor becomes irradiated by the intense X-ray emission from the vicinity of the accretor during outburst, which leads to an increase of the mass outflow from this star, able to keep the disk in the hot state for several years.

We find an increase of the mean $T_{\rm Ceo}$ with $P_{\rm orb}$, hence the disk radius, in the ensemble consisting of both SXTs and DNe (Fig. 9). Although the scatter is appreciable in the systems with long $P_{\rm orb}$, the systems with short $P_{\rm orb}$ are clearly located in a small region of Fig. 9. As given by Warner (1995), the viscous time of the disk $t_\nu \sim r^2/\nu_{\rm k} \sim r/\nu_{\rm rad}$, where $\nu_{\rm k}$ is the coefficient of effective kinematic viscosity of the gas and $\nu_{\rm rad}$ is the radial drift velocity, increases with r. It can yield the observed increase of $T_{\rm Ceo}$ with $P_{\rm orb}$. The observed small $T_{\rm m}/T_{\rm echo}$ (often <1, Table 1) implies that a sufficient amount of the disk matter must be available to bring the disk back to the hot state after the end of the main outburst. Most systems in Table 1 for which q is known have a similar small $q \approx 0.1$, which allows the tidal instability of the disk. Tidal forces are thus a viable mechanism for the transfer of matter through the cold outer disk region between the echo outbursts (Hellier 2001; Truss et al. 2002), but further time dependent modeling is needed, especially for the disk configuration in KS 1731–260.

The position of KS 1731–260 in Fig. 9 corresponds to that occupied by black hole SXTs and indicates the length of its $P_{\rm orb}$ to be at least 5–10 h (definitely longer than in SU UMa DNe). This is an independent support to Revnivtsev & Sunyaev (2003) who estimate from the assumed superorbital cycle that its $P_{\rm orb}$ is exceptionally long, 1–3 d. Indeed, the length of $P_{\rm orb} \approx 1$ d is consistent with the correlation in Fig. 9.

In summary, the behavior of KS 1731–260 appears to be a fascinating example of the time evolution of a system with a unique configuration of the disk, i.e. a thermally stable inner region surrounded by a thermally unstable outer annulus. Modeling of time evolution of such a system in case of a variable $\dot{m}_{\rm tr}$ and assessment of the role of tidal forces and irradiation of the disk in this configuration is very promising. It will yield important results for our understanding of mass-accreting compact objects.

Acknowledgements. The support by the grant 205/08/1207 of the Grant Agency of the Czech Republic is acknowledged. This research has made use of the observations provided by the ASM/*RXTE* team. I thank Dr. A. Henden for information on some dwarf novae from the AAVSO International database. I thank Prof. P. Harmanec for providing me with the code HEC13. The Fortran source version, compiled version and brief instructions how to use the program can be obtained via http://astro.troja.mff.cuni.cz/ftp/hec/HEC13/

References

Bailyn, Ch. D., & Orosz, J. A. 1995, ApJ, 440, L73
Barret, D., Motch, Ch., & Predehl, P. 1998, A&A, 329, 965
Bath, G. T., & Pringle, J. E. 1981, MNRAS, 194, 967
Callanan, P. J., Garcia, M. R., McClintock, J. E., et al. 1995, ApJ, 441, 786
Campana, S., Stella, L., Gastaldello, F., et al. 2002, ApJ, 575, L15
Campana, S., Ravasio, M., Israel, G. L., et al. 2003, ApJ, 594, L39
Campana, S., Ferrari, N., Stella, L., et al. 2005, A&A, 434, L9
Chakrabarty, D., & Morgan, E. H. 1998, Nature, 394, 346
Chelovekov, I. V., Grebenev, S. A., & Sunyaev, R. A. 2006, AstL, 32, 166
Chevalier, C., & Ilovaisky, S. A. 1994, IAU Circ., 6118
Chen, W., Shrader, C. R., & Livio, M. 1997, ApJ, 491, 312
Deloye, C. J., Heinke, C. O., Taam, R. E., et al. 2008, MNRAS, 391, 1619
Dubus, G., Hameury, J.-M., & Lasota, J.-P. 2001, A&A, 373, 251

Esin, A. A., Lasota, J.-P., & Hynes, R. I. 2000, A&A, 354, 987
Filippenko, A. V., & Chornock, R. 2001, IAU Circ., 7644
Filippenko, A. V., Leonard, D. C., Matheson, T., et al. 1999, PASP, 111, 969
Finger, M. H., Wilson, R. B., & van Paradijs, J. 1996, IAU Circ., 6286
Garcia, M. R., McClintock, J. E., Narayan, R., et al. 1998, in Wild Stars In The Old West, ed. S. Howell, E. Kuulkers, & C. Woodward, ASP Conf. Ser., 137, 506
Goranskij, V. P. 2001, IBVS, 5068, 1
Hameury, J.-M., Menou, K., Dubus, G., et al. 1998, MNRAS, 298, 1048
Hellier, C. 2001, PASP, 113, 469
in 't Zand, J. J. M., Cornelisse, R., Kuulkers, E., et al. 2001, A&A, 372, 916
Jonker, P. G., Mendez, M., Nelemans, G., et al. 2003, MNRAS, 341, 823
Jonker, P. G., Bassa, C. G., Nelemans, G., et al. 2006, MNRAS, 368, 1803
Jonker, P. G., Bassa, C. G., & Wachter, S. 2007, MNRAS, 377, 1295
Kato, T., Stubbings, R., Monard, B., et al. 2004, PASJ, 56, S89
King, A. R. 2006, in Compact Stellar X-Ray Sources (Cambridge Univ. Press)
King, A. R., & Cannizzo, J. K. 1998, ApJ, 499, 348
King, A. R., & Ritter, H. 1998, MNRAS, 293, L42
Leach, R., Hessman, F. V., King, A. R., et al. 1999, MNRAS, 305, 225
Levine, A. M., Bradt, H., Cui, W., et al. 1996, ApJ, 469, L33
Lewin W. H. G., van Paradijs, J., & van den Heuvel, E. P. J. 1995, X-ray Binaries (Cambridge Univ. Press)
Maitra, D., & Bailyn, Ch. D. 2006, ApJ, 637, 992
Mignani, R. P., Chaty, S., Mirabel, I. F., et al. 2002, A&A, 389, L11
Mineshige, S., Tuchman, Y., & Wheeler, J. C. 1990, ApJ, 359, 176
Morrison, R., & McCammon, D. 1983, ApJ, 270, 119
Muno, M. P., Fox, D. W., Morgan, E. H., et al. 2000, ApJ, 542, 1016
Narayan, R., Garcia, M. R., & McClintock, J. E. 1997, ApJ, 478, L79
Nogami, D., Monard, B., Retter, A., et al. 2004, PASJ, 56, L39
Nowak, M. A., Heinz, S., & Begelman, M. C. 2002, ApJ, 573, 778
Orosz, J. A., Bailyn, C. D., & Whitman, K. 2001a, ATel, 75
Orosz, J. A., Kuulkers, E., van der Klis, M., et al. 2001b, ApJ, 555, 489
Orosz, J. A., Groot, P. J., van der Klis, M., et al. 2002, ApJ, 568, 845
Patterson, J., Kemp, J., Skillman, D. R., et al. 1998, PASP, 110, 1290
Patterson, J., Masi, G., Richmond, M. W., et al. 2002, PASP, 114, 721
Pavlenko, E. P., Shugarov, S. Yu., Katysheva, N. A., et al. 2006, Binary Stars as Critical Tools and Tests in Contemporary Astrophysics, held 22–25 August, 2006 in Prague, Czech Republic, IAU Symp., 240, 89
Powell, C. R., Haswell, C. A., & Falanga, M. 2007, MNRAS, 374, 466
Revnivtsev, M., & Sunyaev, R. 2003, A&A, 399, 699
Ritter, H., & Kolb, U. 2003, A&A, 404, 301
Robinson, E. L., Ivans, I. I., & Welsh, W. F. 2002, ApJ, 565, 1169
Roelofs, G. H. A., Groot, P. J., Benedict, G. F., et al. 2007a, ApJ, 666, 1174
Roelofs, G. H. A., Groot, P. J., Nelemans, G., et al. 2007b, MNRAS, 379, 176
Rutledge, R. E., Bildsten, L., Brown, E. F., et al. 2001, ApJ, 559, 1054
Shih, I. C., Bird, A. J., Charles, P. A., et al. 2005, MNRAS, 361, 602
Shirey, R. E., Bradt, H. V., Levine, A. M., et al. 1996, ApJ, 469, L21
Šimon, V. 2000, A&A, 354, 103
Šimon, V. 2002, A&A, 381, 151
Šimon, V. 2003, A&A, 405, 199
Šimon, V. 2004, A&A, 418, 617
Šimon, V. 2008, A&A, 492, 135
Skidmore, W., Welsh, W. F., Wood, J. H., et al. 1997, MNRAS, 288, 189
Syunyaev, R., Gilfanov, M., Churazov, E., et al. 1990, SvAL, 16, 59
Steeghs, D., Howell, S.B., Knigge, C., et al. 2007, ApJ, 667, 442
Szkody, P. 1987, ApJS, 63, 685
Szkody, P., Henden, A., Agueros, M., et al. 2006, AJ, 131, 973
Truss, M. R., Wynn, G. A., Murray, J. R., et al. 2002, MNRAS, 337, 1329
Uemura, M., Kato, T., Ishioka, R., et al. 2002, PASJ, 54, L79
Vogt, N. 1980, A&A, 88, 66
Vondrák, J. 1969, Bull. Astron. Inst. Czechosl., 20, 349
Vondrák, J. 1977, Bull. Astron. Inst. Czechosl., 28, 84
Warner, B. 1995, Cataclysmic Variable Stars (Cambridge: Cambridge Univ. Press)
Webb, N. A., Naylor, T., Ioannou, Z., et al. 2000, MNRAS, 317, 528
Whittaker, E., & Robinson, G. 1946, The Calculus of Observations (London: Blackie & Son Ltd), 303
Wijnands, R. 2002, in The High Energy Universe at Sharp Focus: Chandra Science, ed. E. M. Schlegel, & S. Vrtilek (San Francisco: ASP), ASP Conf. Ser., 262 [arXiv:astro-ph/0107600]
Wijnands, R. 2006, Trends in Pulsar Research, ed. J. A. Lowry (New York, USA: Science Publishers, Inc.), 53
Wijnands, R. A. D., & van der Klis, M. 1997, ApJ, 482, L65
Wijnands, R., Miller, J. M., Markwardt, C., et al. 2001a, ApJ, 560, L159
Wijnands, R., Mendez, M., Markwardt, C., et al. 2001b, ApJ, 560, 892
Wijnands, R., Heinke, C. O., & Grindlay, J. E. 2002a, ApJ, 572, 1002
Wijnands, R., Guainazzi, M., van der Klis, M., et al. 2002b, ApJ, 573, L45
Zurita, C., Sanchez-Fernandez, C., Casares, J., et al. 2002, MNRAS, 334, 999